THE EFFECT OF WATER TEMPERATURE ON COOLING DURING HIGH PRESSURE WATER DESCALING

Michal POHANKA [a,*]***, Helena VOTAVOVÁ*** [a]***, Miroslav RAUDENSKÝ*** [a]***,***
Jong Yeon HWANG [b]***, Jong Woo YOU*** [b]***, Sang Hyeon LEE*** [b]

[a] Heat Transfer and Fluid Flow Laboratory, Faculty of Mechanical Engineering,
Brno University of Technology, Brno, Czech Republic

[*] Email: Michal.Pohanka@vut.cz

[b] POSCO Gwangyang Work, Gwangyang-si, Jeonnam, Korea

Production of hot rolled steel plates is connected with high temperatures at which steel reacts with oxygen in the atmosphere and oxide layers (scales) are formed on the surface. Scales affect the surface quality of the product and must be eliminated before the product enters any further rolling operations. The scales are usually removed by high pressure flat jet water nozzles in a process called hydraulic descaling. One side effect of this form of descaling is intense cooling of the product, which runs counter to the purpose of descaling. One way to decrease this effect is to use water at higher temperatures. Laboratory experiments were performed in order to determine the degree of influence of water temperature on the intensity of cooling. Temperature measurements were used as an input for inverse algorithm calculations and heat transfer coefficient determinations. The variables were computed as a function of time and position. The results were compared and significant decrease in the cooling intensity was observed. The findings are discussed in detail.

Key words: *nozzle, high pressure, descaling, water temperature, cooling, heat transfer coefficient*

1. Introduction

Steel production in continuous rolling mills is a major method of steel production. Usually, the semi-finished casting product (slab, bloom or ingot) is heated to a high temperature and fed into the rolling mill. Due to the high temperature and surrounding atmosphere, oxides are formed on the surface of the product and are generally called scales. These scales are mainly würstite (FeO), hematite (Fe_2O_3) and magnetite ($FeO \cdot Fe_2O_3$). Scales form a thin layer on the surface of the product and significantly affect the quality of the rolled material [1]. To properly fabricate the hot rolled product all of the scales must be eliminated from the surface before the product enters rolling operations [2].

One of the most promising and widely used technologies for scale removal is a descaling box, which is basically a row of flat jet high pressure nozzles [3]. The nozzles are arranged on spray headers. The descaler usually uses a working pressure between 8 to 45 MPa. The nozzles are usually designed so that the descaling operation is optimal from a descaling point of view. One important side effect of this design is that it causes intense cooling of the product. A heat flux of over 20 MWm^{-2} can be created very easily [4]. Optimal conditions for hot rolled steel exist when the product maintains a

stable, homogeneous temperature along the steel strip. The temperature shock caused by the water from the nozzles is in most cases undesirable and must be effectively suppressed.

In recent years, developments and new trends in high pressure water descaling have focused on the reduction of the nozzle sizes and has allowed for the distance between the nozzles and the heated product to be lowered. High pressure flat jet nozzles can reach a spray depth from 1.5 to 3 mm at a nozzle standoff below 100 mm, which leads to a concentration of energy in a smaller area and results in higher descaling efficiency [5]. This improves the effectiveness of the descaler and more attention can be paid to the reduction of the cooling of the product.

Industry and research teams usually identify several parameters that can affect descaling performance, including several angles and nozzle distances [6] or nanoparticles presented in water [7]. Even the structure of the oxidized surface plays important role in the process [9]. Yet every study assumes the temperature of sprayed water as a fixed variable. Our study examines this aspect for a given descaling nozzle with a widely used configuration that is believed to be close to an optimal setting. Nine measurements were taken for water temperatures between 20 °C and 50 °C.

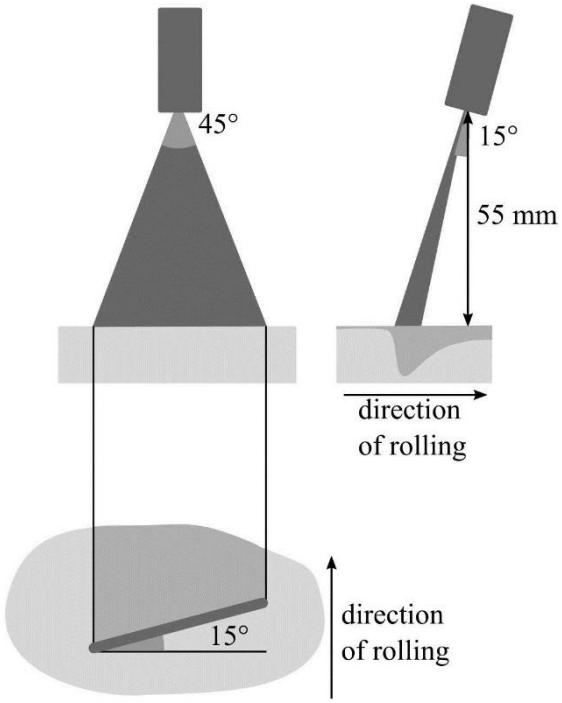

Fig. 1. Tested configuration

2. Experiments

The configuration of nozzle is illustrated in fig. 1. Nozzle is producing 58 l/min at 40 MPa and has a 45° spray angle. Tested configuration was as follows:

- 55 mm spray height,
- 40 MPa water pressure,
- 15° offset angle,
- 15° inclination angle.

The nozzle has a theoretical footprint approximately 47 mm long.

The experiments were performed on a laboratory experiment stand that is used for tests with moving samples. The stand is illustrated in fig. 2. The sample was a stainless steel (1.4828) plate which was 25 mm thick. A thermocouple was installed inside the plate 0.6 mm under the surface and the thermocouple wire was placed parallel to the descaled surface. The details of the built-in thermocouple are described in [10]. The tested sample was installed on a moving carriage and insulated from the uncooled side. The tested sample was heated in an electric heater for a given time to 950 °C in a non-oxidizing (nitrogen) atmosphere. When the temperature in the specimen reached the desired value, the data logger began to record the temperature from the thermocouple and the corresponding position of the carriage. The hot sample was placed into the upper position and then moved along the support frame under the spray nozzles at 0.5 m/s. Built-in thermocouple passed directly under the spraying nozzle. Data from the experiment was collected from the data logger after the experiment was complete.

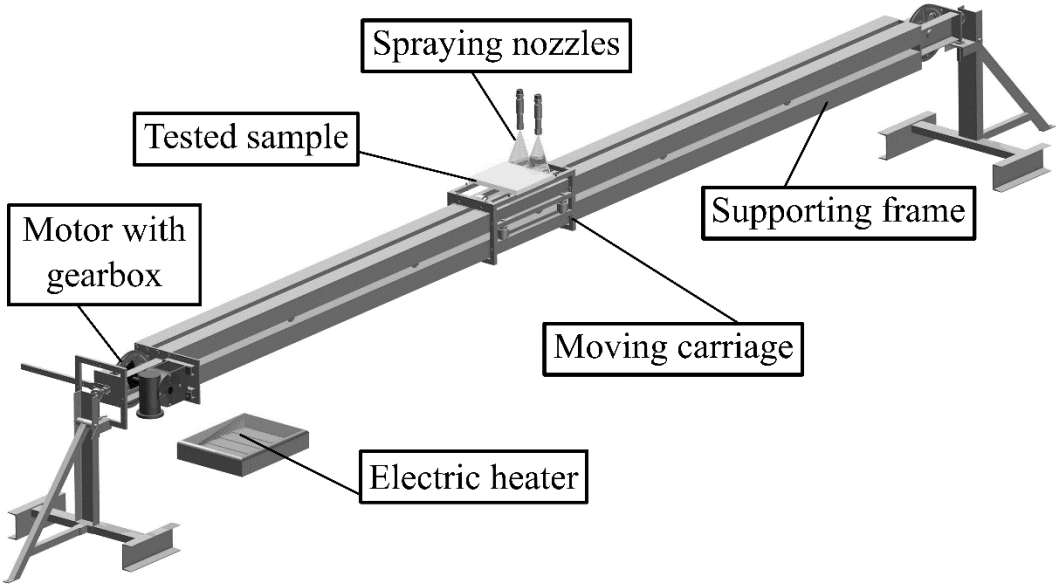

Fig. 2. Experimental stand used for tests with moving samples

There were 9 experiments in total. The plan of the experiments is summarized in the Tab. 1. The water temperature was set from 20 °C up to 50 °C with equidistant step of 10 °C. Measurement was repeated three times for the lowest water temperature and two times for elevated temperature levels.

Tab. 1. Experiment plan

Experiment	E1	E2	E3	E4	E5	E6	E7	E8	E9
Water temperature [°C]	20	20	20	30	30	40	40	50	50

3. Evaluation of boundary conditions

The main step in the evaluation of the measured data is the inverse heat conduction task. The temperature distribution inside the tested specimen follows the heat diffusion equation (1) (parabolic partial differential equation) together with the initial condition (2), the boundary condition at the free surface (3) and boundary condition at the insulated built-in surfaces (4) [11].

$$k\left[\frac{\partial^2 T(x,y,z,t)}{\partial x^2}+\frac{\partial^2 T(x,y,z,t)}{\partial y^2}+\frac{\partial^2 T(x,y,z,t)}{\partial z^2}\right]=\rho c\frac{\partial T(x,y,z,t)}{\partial t}, \qquad \begin{matrix}(x,y,z)\in\Omega,\\ t\in\mathbb{R}_0^+\end{matrix} \qquad (1)$$

$$T(x,y,z,t_0)=f(x,y,z), \qquad (x,y,z)\in\Omega \qquad (2)$$

$$-k\left[\frac{\partial T(x,y,z,t)}{\partial n}\right]\Big|_{(x,y,z)=(x_0,y_0,z_0)}=h(x_0,y_0,z_0,t)\,[T_\infty-T(x_0,y_0,z_0,t)], \qquad (x_0,y_0,z_0)\in\partial\Omega_1 \qquad (3)$$

$$\frac{\partial T(x,y,z,t)}{\partial n}\Big|_{(x,y,z)=(x_1,y_1,z_1)}=0, \qquad (x_1,y_1,z_1)\in\partial\Omega_2 \qquad (4)$$

where T is the temperature of the specimen as a function of space coordinates x, y, z and time t, k is for the thermal conductivity of the specimen, c is for the thermal capacity of the specimen and ρ is for the density of the specimen. Set Ω is the domain where the problem is set and $\partial\Omega$ is its boundary (surface of the specimen), which is divided into $\partial\Omega_1$, where the convective heat flux occurs, and $\partial\Omega_2$, where the insulation around the specimen is placed. Vector n is the unit normal vector at the boundary $\partial\Omega$. Function f(x,y,z) defines the initial state at initial time t_0. Temperature T_∞ defines the temperature of the sprayed water.

The heat equation can be solved analytically only for a very limited range of initial and boundary conditions. Nevertheless, the solution can be approached numerically with sufficient precision [12]. Inverse problems represent a task of an order of magnitude harder than directly solving the equation. The objective is to compute the boundary condition (3) from a given set of measurements of thermocouples inside the domain, more specifically by computing the heat transfer coefficient as a position and time dependent variable. As a byproduct of the computation, surface temperatures and transferred heat are computed.

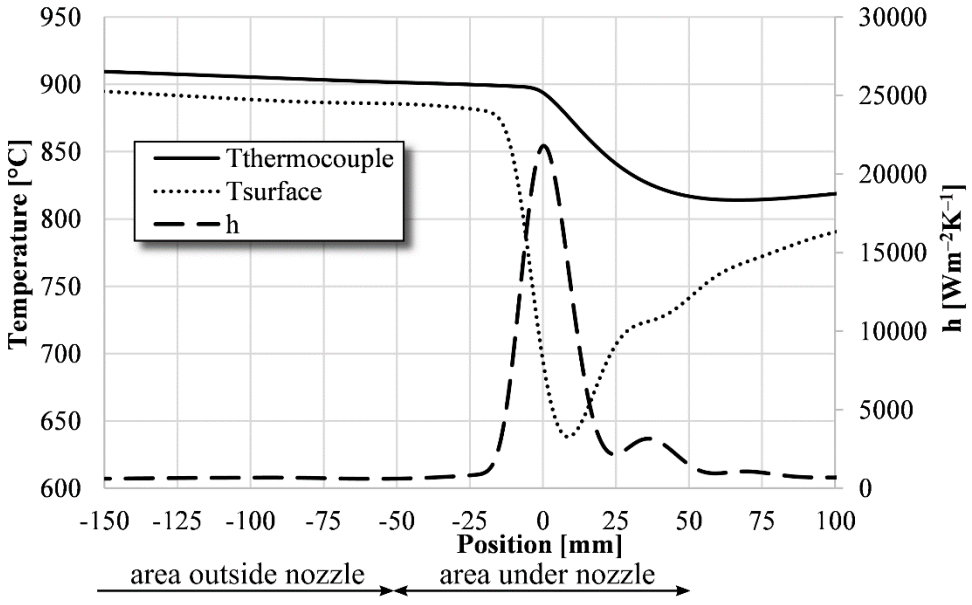

Fig. 3. Typical outcome of the experiment: measured temperature by the thermocouple, computed temperature at the surface and corresponding heat transfer coefficient.

The inverse heat conduction task is a mathematically ill-posed problem and can sometimes be very sensitive to errors in input data. The values of heat transfer coefficient on the surface above the thermocouple are computed iteratively with respect to time. The sequential identification inverse method is used to stabilize the computation, which is described in detail in [13] and which is based on sequential estimates of the time varying boundary condition and usage of future time steps. The algorithm uses forward solver of the heat transfer problem and computes the response temperature at the thermocouple position for linearly changing heat transfer coefficient in several time steps. To determine the boundary condition and heat transfer coefficient for given position, the measured temperatures from the thermocouple are compared with computed temperatures from the model. The slope of linearly changing heat transfer coefficient is changed until the mean square error of the temperatures in the computed section of the time steps is minimized. When the optimal slope of heat transfer coefficient is found the forward solver is used to compute temperature field in the next time step using the computed boundary conditions. A typical outcome of the experiment is shown in fig. 3.

Due to the limited speed of propagation of the information of the cooling impulse in the specimen, the temperature change is measured at the thermocouple with some delay (see fig. 3). This causes blurring of the information of the surface temperature and also blurring of the heat transfer coefficient with respect to the time scale. This in practice means that the peak of the heat transfer coefficient as a function of time tends to be underestimated and the lap of intensive cooling impulse tends to be overestimated. The algorithm compensates for this blurring by the second peak in the outgoing area. It is important to note that this second peak has no physical meaning. Due to this bias of outcomes it is not appropriate to compare the results coming from these experiments with numerical simulations, however it is possible to compare the results among the experiments.

The numerical simulations can report an average heat transfer coefficient in range from 10 $kWm^{-2}K^{-1}$ up to 110 $kWm^{-2}K^{-1}$ [14]. The experimental work of research teams can report values from 17.65 $kWm^{-2}K^{-1}$ to 19.9 $kWm^{-2}K^{-1}$ [15], but also from 270 $kWm^{-2}K^{-1}$ to 430 $kWm^{-2}K^{-1}$ [16] for similar rolling conditions and similar configurations. This illustrates the variability of the outcomes from different research teams.

4. Results of the experiments and discussion

Corresponding heat transfer coefficients were computed for all configurations as a position dependent variable where the position is in the direction of plate movement. The measured temperatures are presented in fig. 4. Computed temperatures for position at the surface of the specimen are shown in fig. 5. The profiles of the outcomes are compared in fig. 6 and in detail in fig. 7. The highest peak is located at value 0 (i.e. right in the middle of the direct impact of the water stream). All the position dependent heat transfer coefficients show more or less the same dependency on the position. The biggest difference was observed under the nozzle in the vicinity of the zero value. The computed maximum of all the experiments reached values from 20 $kWm^{-2}K^{-1}$ up to 25 $kWm^{-2}K^{-1}$.

For each profile the average value of heat transfer coefficient under direct impact and heat transfer coefficient outside direct impact was computed. Average heat transfer coefficient under direct impact is computed as an arithmetic average value of the curve of heat transfer coefficient from position -50 mm to position 50 mm, average heat transfer coefficient outside the direct impact is computed as an average value of the curve of heat transfer coefficient for the positions from -150 mm to -50 mm.

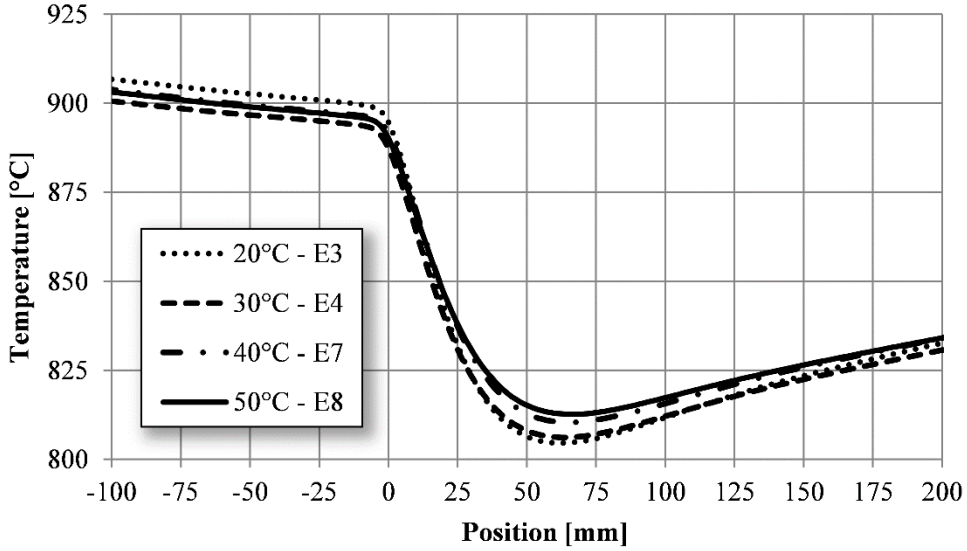

Fig. 4. Measured temperatures by the thermocouple

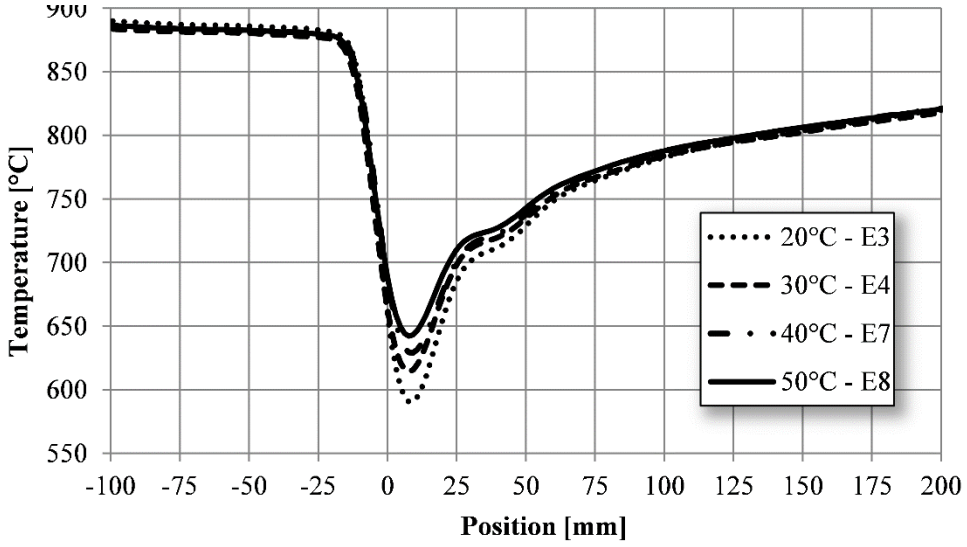

Fig. 5. Computed temperatures at the surface of the specimen

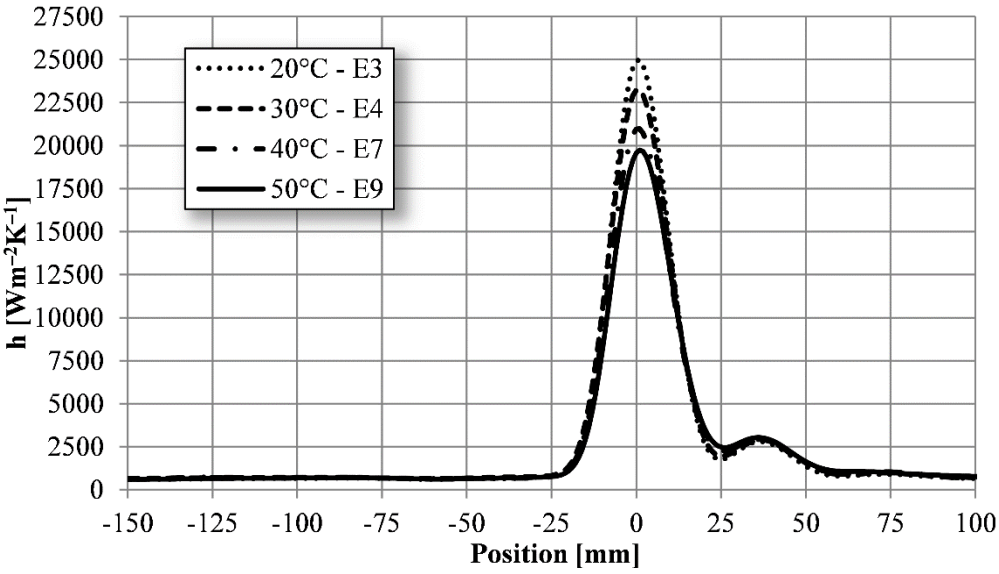

Fig. 6. Heat transfer coefficient for different water temperature

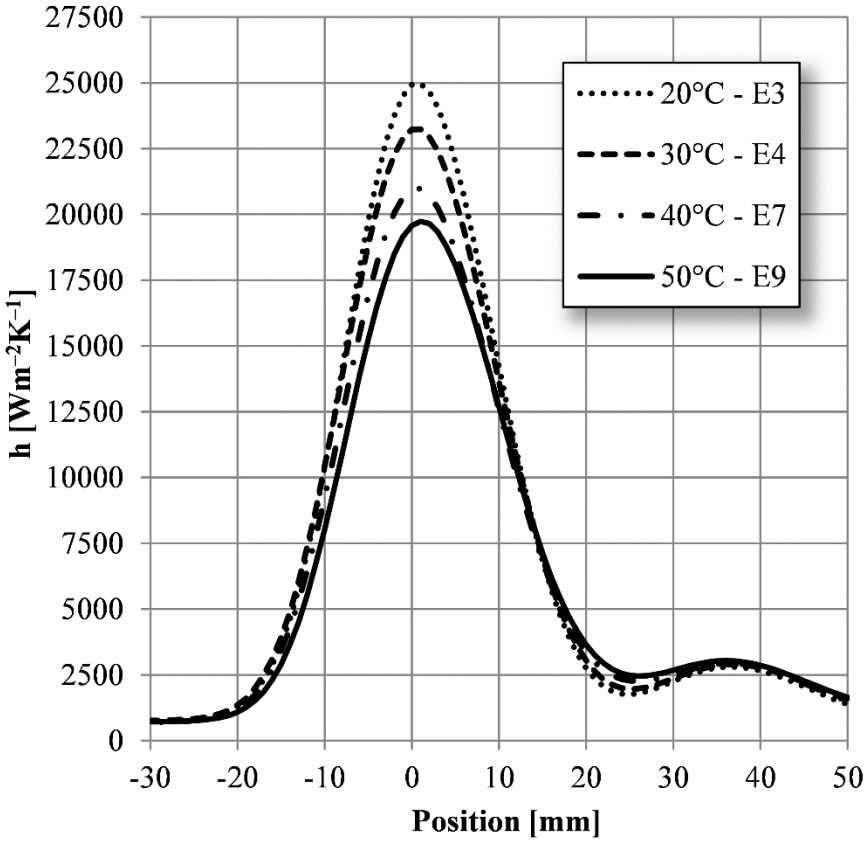

Fig. 7. Heat transfer coefficients for different water temperature - detail

The values of heat transfer coefficient under the direct impact and outside the direct impact are for each experiment summarized in tab. 2. Linear regression was used for the data analysis and the significance level of the statistical tests was set to 0.05. The corresponding p-value for the linear coefficient was computed to be 0.50. Because the p-value is greater than the significance level, it suggests that the observed data is not linearly dependent and the water temperature had no significant effect on the cooling intensity in the area before direct impact of the water jet on the surface.

Tab. 2. List of heat transfer coefficient tests and the average heat transfer coefficients measured for various water temperatures

Experiment	Water temperature [°C]	Average heat transfer coefficient under direct impact [$Wm^{-2}K^{-1}$]	Average heat transfer coefficient outside direct impact [$Wm^{-2}K^{-1}$]
E1	20	6124	420
E2	20	6168	455
E3	20	6049	361
E4	30	5905	395
E5	30	6024	352
E6	40	5652	375
E7	40	5479	386
E8	50	5368	371
E9	50	5278	413

On the other hand, the cooling intensity under the nozzle was significantly affected by the water temperature. The regression equation was computed to be

$$h = -27.23 \cdot T + 6691 \quad (5)$$

with heat transfer coefficient h set in [$Wm^{-2}K^{-1}$] and water temperature in [°C]. The coefficient of determination was 0.93. The dependence is illustrated in fig. with the corresponding measured points and with 95% confidence intervals and a 95% prediction interval. A 95% confidence interval shows the range in which the estimated mean heat transfer coefficient for a given temperature is expected to fall with 95% probability. A 95% prediction interval is the range in which the predicted heat transfer coefficient for a new observation is expected to fall with 95% probability. The function shows that by increasing the water temperature from 20 °C to 50 °C the average heat transfer coefficient under the nozzle can be reduced by up to 13.3%.

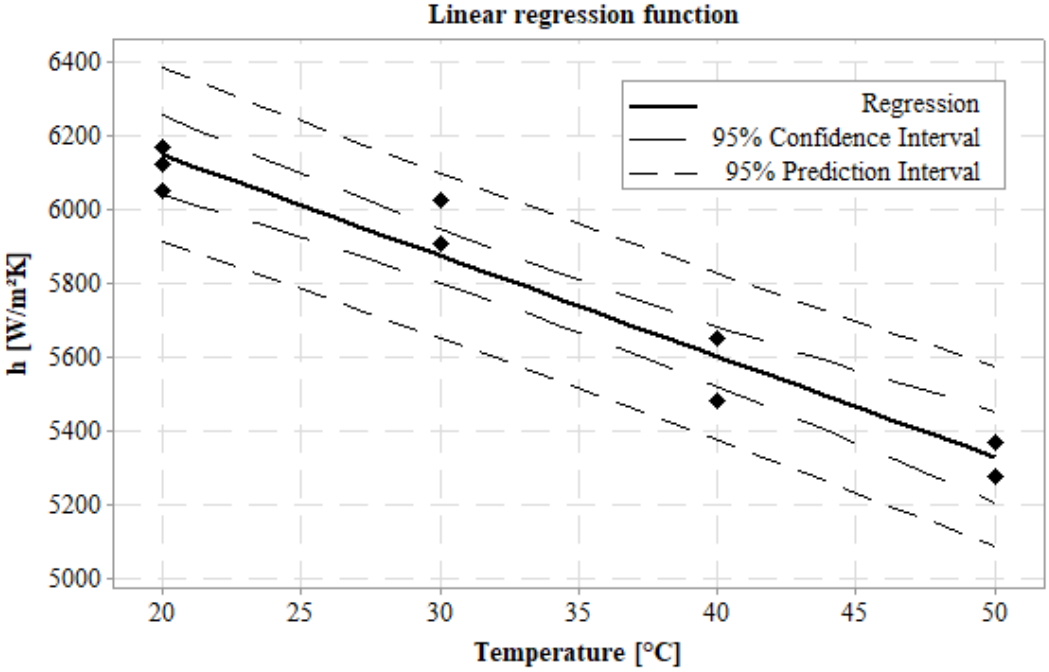

Fig. 8. Graph of the regression function with confidence interval and prediction interval.

5. Conclusion

The experiments were designed in order to prove whether water temperature plays an important role in the cooling intensity in hydraulic descaling. The water temperature varied from 20 °C to 50 °C. The position dependent heat transfer coefficient was represented by the average value in an area of ±50 mm around the nozzle. These average values were used for the linear regression model. The dependency was significant and the estimated decrease was approximately 27.23 $Wm^{-2}K^{-1}$ for a 1 °C increase in water temperature. The function shows that by increasing the water temperature from 20 °C to 50 °C the average heat transfer coefficient under the nozzle can be reduced by up to 13.3%. The dependency of the average heat transfer coefficient outside the direct impact area was not significant on the water temperature. This fact is supported by the fact that the dominant cooling mechanism in this area is the evaporation of small water droplets. The heating of the water from the set temperature to the boiling point occurs in the area of direct impact rather than in the area outside the direct impact.

Acknowledgements

The research leading to these results has received funding from the MEYS under the National Sustainability Programme I (Project LO1202) and by the internal grant of the Brno University of Technology focused on specific research and development No. FSI-S-17-4346.

Nomenclature

c	Thermal capacity, [$Jkg^{-1}K^{-1}$]
h	Heat transfer coefficient, [$Wm^{-2}K^{-1}$]
k	Thermal conductivity, [$Wm^{-1}K^{-1}$]
n	Unit normal, []
t	Time, [s]
t_0	Initial time, [s]
T	Temperature, [°C]
T_∞	Water temperature, [°C]

Greek symbols

ρ	Density, [$kg\,m^{-1}$]
Ω	Domain, [m×m×m]
$\partial\Omega$	Boundary of the domain Ω, [m×m]
$\partial\Omega_1$	Boundary of the domain Ω, free surface [m×m]
$\partial\Omega_2$	Boundary of the domain Ω, insulated surface [m×m]

References

[1] Hrabovský, J., Horský J., Numerical simulation of the high pressure hydraulic descaling, *Proceedings Metal 2010.* 19th International Metallurgical and Materials Conference, Rožnov pod Radhoštěm, Czech Republic, 2010, pp. 621–626

[2] Kotrbáček, P., *et al.*, Optimization of working roll cooling in hot rolling, *9th International Conference on Heat Transfer, Fluid Mechanics and Thermodynamics*, Associazione Italiana di metallurgia, Milano, Italy, 2013, pp. 1–11

[3] Pohanka, M., Two-dimensional correction of data measured using a large pressure sensor, *Computational Methods and Experimental Measurements XI*, Eleventh International Conference on Computational Methods and Experimental Measurements, London, UK, 2003, Vol. 4, pp. 587-595

[4] Hnízdil, M., Raudenský M., Descaling by pulsating water jet, *Proceedings Metal 2010*, 19th International Metallurgical and Materials Conference, Rožnov pod Radhoštěm, Czech Republic, 2010, pp. 209–213

[5] Frick, J. W., Enhanced Accuracy of Descaling Nozzle Arrangements With New, Complementary Measurement Methods, *AISTech - Iron and Steel Technology Conference Proceedings*, AISTech - The Iron & Steel Technology Conference and Exposition, Indianapolis, USA, 2014, Vol. 2, pp. 2025-2028

[6] Farrugia, D., *et al.*, Advancement in understanding of descalability during high pressure descaling, *Key Engineering Materials*, 622-623 (2014), pp. 29-36, DOI: 10.4028/www.scientific.net/KEM.622-623.29

[7] Mangrulkar, C. K., *et al.*, Experimental Investigation of Convective Heat Transfer Enhancement Using Alumina/Water and Cooper Oxide/Water Nanofluids, *Thermal Science*, 20 (2016), 5, pp. 1681-1692

[8] Hussein, A. M., *et al.*, Heat Transfer Enhancement with Elliptical Tube Under Turbulent Flow TiO2-Water Nanofluid, *Thermal Science*, 20 (2016), 1, pp. 89-97

[9] Ge, M., Numerical Investigation of Flow Characteristics Over Dimpled Surface, *Thermal Science*, 20 (2016), 3, pp. 903-906

[10] Pohanka, M., Horský, J., Inverse algorithms for time dependent boundary reconstruction of multidimensional heat conduction model, *Proceedings* (Josef Leja), THERMOPHYSICS 2007, Kočovce, Slovakia, 2007, pp. 14-23

[11] Bergman, T. L., *et al.*, *Fundamentals of heat and mass transfer (7th edition),* John Wiley and Sons Inc., New York, USA, 2011

[12] He, Y., *et al.* A Novel Numerical Method for Heat Equation, *Thermal Science*, 20 (2016), 3, pp. 1018-1021

[13] Pohanka, M., Kotrbáček, P., Design of Cooling units for Heat Treatment, in: *Heat Treatment - Conventional and Novel Applications* (Dr. Frank Czerwinski), InTechOpen, Rijeka, Croatia, 2012, pp. 1-20, DOI: 10.5772/50492

[14] Gao P., Study of Convective Heat Transfer Coefficient of High Pressure Water Descaling, *Applied Mechanics and Materials*, 599-601 (2014), pp. 1976-1980, DOI: 10.4028/www.scientific.net/AMM.599-601.1976

[15] Čarnogurská, M., *et al.*, Thermal effects of a high-pressure spray descaling process, *Materiali in tehnologije = Materials and technology*, 48 (2014), 3, pp. 389-394

[16] Choi, J. W, Choi, J.W., Convective Heat Transfer Coefficient for High Pressure Water Jet, *ISIJ International*, 42 (2002), 3, pp. 283-289, DOI: 10.2355/isijinternational.42.283